Overall the D2cc values for the OAR have a lower percentage difference between planners than the D0.1cc due to the increased influence within the small volume.
Conclusions: T2 MR imaging alone for reconstruction, using the external applicator surface, is reproducible between different planners. Slice thickness and inter-space gap are known parameters that can lead to uncertainties in applicator reconstruction, but by using mutual information from orthogonal sequences these uncertainties can be minimised.
The changes in DVH parameters between planners are small, for both HR-CTV and all OARs, and would not result in a clinically significant change in terms of optimisation approach for the treatment plan.

OC-0179
MR guided brachytherapy for cervical cancers using a novel titanium applicator and a novel MR sequence
S. Petit[1], P. Wielopolski[2], R. Rijnsdorp1[1], J. Mens[1], I. Kolkman-Deurloo[1]
[1]Erasmus Medical Center Rotterdam, Department of Radiation Oncology, Rotterdam, The Netherlands
[2]Erasmus Medical Center Rotterdam, Department of Radiology, Rotterdam, The Netherlands

Purpose/Objective: For brachytherapy of cervical cancers, the imaging modality of choice for delineation of targets and organ at risks (OAR) is T2-weighted MR imaging. Applicator reconstruction using MR imaging can be problematic for applicators composed of titanium. Titanium generates susceptibility artefacts on MR scans, causing signal voids near the titanium that may hamper applicator reconstruction. The goal of this study is to propose a novel MR sequence that yields non-deformed, high resolution and high contrast images that can be used for accurate and reproducible reconstruction of titanium applicators. The method is tested using a new design of the tandem and ovoid titanium Rotterdam applicator (Nucletron).
Materials and Methods: A 1.5 Tesla MR scanner was used with a 3D radiofrequency Spoiled Gradient Recalled Echo sequence (SPGR, TE: 1.1 ms, TR: 2.5, voxel size: 1.4x1.4x1.6 mm^3, flip angle: 3°, number of excitations: 3) for imaging and applicator reconstruction. The geometrical accuracy of the applicator in the images was assessed using an in house developed gel filled phantom that could fixate the applicator. The inter-observer variability of applicator reconstruction was studied by analysing the results of eight different technicians that each performed applicator reconstruction for four different patients. The rigidity of the applicator allowed the use of a single library applicator, a digital model of the applicator with fixed dimensions, for applicator reconstruction.
Results: On a standard T2 weighted scan, the titanium did not produce artefacts that hampered tumour delineation, but the contrast between the applicator and uterus was not sufficient for accurate applicator reconstructions. The 3D SPGR scan sequence yielded an excellent contrast between the soft tissues and the applicator, which was clearly visible as a signal void. When the intra-uterine was aligned with the B0 field,the width (FWHM) of its signal void was exactly equal to the real diameter of 3.0 mm, but it increased to 6.2 mm when the intra-uterine was tilted 46°compared to the B0 field. Because the intra-uterine tube was located in the centre of the signal void (within 0.7 mm), the accuracy of applicator reconstruction was not affected by the expansion of the signal void for large tilt angles.This was confirmed by the excellent inter-observer variability among the eight technicians. The mean deviation for all reconstructed dwell positions was smaller than 1.0 mm and the maximum deviation of any dwell position among all patients and technicians was only 1.7 mm.
Conclusions: The titanium applicator was clearly visible on the 3D SPGR MR images, allowing applicator reconstruction with excellent accuracy and reproducibility. When used in addition to the standard T2 weighted MR images for tumour and OAR delineation, high accuracy MR guided brachytherapy is feasible with a titanium applicator.

OC-0180
CT and MRI based seed localization in post-implant evaluation of permanent prostate brachytherapy
M. De Brabandere[1], B. Al-Qaisieh[2], L. De Wever[3], K. Haustermans[1], C. Kirisits[4], M.A. Moerland[5], R. Oyen[3], A. Rijnders[6], F. Van den Heuvel[1], F.A. Siebert[7]
[1]University Hospital Gasthuisberg, Dept of Radiation Oncology, Leuven, Belgium
[2]St James's Institute of Oncology, Dept. of Medical Physics and Engineering, Leeds, United Kingdom
[3]University Hospital Gasthuisberg, Dept. of Radiology, Leuven, Belgium
[4]Medical University of Vienna, Dept. of Radiotherapy, Vienna, Austria
[5]University Medical Center Utrecht, Dept. of Radiation Oncology, Utrecht, The Netherlands
[6]Europe Hospitals, Dept. of Radiation Oncology, Brussels, Belgium
[7]University Hospital of Schleswig-Holstein, Dept. of Radiation Oncology, Kiel, Germany

Purpose/Objective: To compare the uncertainties of CT and MRI-T1 based seed reconstruction in post-implant evaluation of permanent prostate brachytherapy in terms of interobserver variability, and to quantify the impact of this seed detection variability on a selection of dosimetric parameters for three postplan techniques: 1) CT only, 2) MRI-T1 fused with MRI-T2, and 3) CT fused with MRI-T2.
Materials and Methods: Seven physicists reconstructed the seed positions on post-implant CT and MRI-T1 weighted images of three patients treated with I-125 seed brachytherapy. A reference seed set was defined by two experienced physicists. The reconstructed seeds were assigned to the reference seeds within an acceptance diameter of 15mm, using a dedicated Matlab program. For each patient and imaging modality the interobserver variability was calculated with respect to the reference (1 SD_{ref}). The effect of this variability on dosimetry (D_{90}, V_{100}, V_{150}) was calculated for CT and for CT + MRI-T2 (both techniques using CT based seed reconstruction), as well as for MRI-T1 + MRI-T2 (using MRI-T1 based seed reconstruction), for a fixed CT and MRI-T2 prostate contour. Contouring was done by two experienced uro-radiologists based on the post-implant CTV-P(rostate) definition according to the ESTRO/EAU/EORTC prostate recommendations.
Results: For CT, on average 98 % of the reconstructed seeds could be assigned to a reference seed, while the mean seed assignment rate for T1 was 93 %. Averaged over three patients, the interobserver variability in CT based seed reconstruction was 1.1 mm (1 SD_{ref}). This resulted in D_{90} variabilities < 2% (1 SD_{ref}) for CT and CT + MRI-T2, which is clinically acceptable (see table). Also the interobserver variabilities in V_{100} and V_{150} were small, with patient mean SD_{ref} values < 1% and < 4% respectively.
The mean interobserver variability in MRI based seed reconstruction was 3.0 mm (1 SD_{ref}). This would be even larger if non-assigned seeds (outside the acceptance diameter) would be taken into account. The larger seed detection uncertainties on MRI-T1 compared to CT are due to the lack of an automated seed finder tool, and the fact that seeds are less clearly depicted on MRI. The impact of the interobserver variability on D_{90} was 6.6% for MRI-T1 + MRI-T2.
Conclusions: Seed reconstruction on MRI-T1-weighted images was less accurate than on CT. This difference in uncertainties should be taken into account and weighted against uncertainties due to contouring and image fusion when comparing the overall reliability of postplan techniques.
Table: Interobserver variability in seed reconstruction (averaged over three patients), expressed as (a) positional deviation (mm) and (b) dosimetric impact (%) with respect to the reference values.

SD_{ref} in seed reconstruction (mm)	CT	MR-T1
	1.1 mm	3.0 mm
SD_{ref} in dosimetry (%)	CT	CT + MR-T2	MR-T1 + MR-T2
D90	1.5	1.3	6.6
V100	0.9	0.5	2.8
V150	3.6	3.2	8.1

OC-0181
Dual energy CT facilitates LDR brachytherapy seed metal artefact reduction
G. Landry[1], B. Reniers[1], E. Vigneault[2], L. Beaulieu[2], J. Wildberger[3], F. Verhaegen[1]
[1]MAASTRO Clinic, Physics, Maastricht, The Netherlands
[2]Centre Hospitalier Universitaire de Québec L'Hôtel-Dieu de Québec, Radiation Oncology, Quebec, Canada
[3]Maastricht University Medical Center (MUMC), Radiology, Maastricht, The Netherlands

Purpose/Objective: The current clinical low dose rate (LDR) brachytherapy dosimetry protocol for low energy photons, AAPM TG43, ignores the effects of tissue composition. Given the photoelectric effect's dominance at the low photon energies, the dosimetry is dependent on the elemental composition and density of tissues. AAPM TG186 recently recommended that brachytherapy dose calculations take heterogeneities into account by using CT images. In LDR seed implants, metal streaking artefacts degrade density (ρ) information and limit the applicability of heterogeneity corrections. Metal artefact reduction (MAR) techniques have been presented, but are currently not clinically implemented in radiotherapy, possibly due to their complexity. Dual energy CT (DECT) imaging allows the reconstruction of mono energetic attenuation maps over a range of diagnostic energies. It has recently been shown that by carefully

choosing this mono-energy, it is possible to achieve MAR in patients with hip prostheses. This approach is simple and easy to implement.The goal of this study is to assess the MAR capacity of DECT in the context of LDR seed implants. More specifically, we aim to ascertain whether the use of DECT can yield dose calculations whose accuracy is not marred by metal artefacts.

Materials and Methods: DECT imaging at 100 kVp and 140 kVp was performed on an ultrasound phantom designed for prostate implants containing inert LDR brachytherapy seeds. The magnitude of artefacts was evaluated as a function of mono-energetic attenuation maps by comparing the standard deviation (σ) in a region of interest (ROI) containing artefacts and one free of artefacts. The ROIs exclude the high signal from the seeds themselves. Additionally, the same analysis was performed on the density map obtained from the standard DECT ρ-Z decomposition which provides a density map directly.

Results:

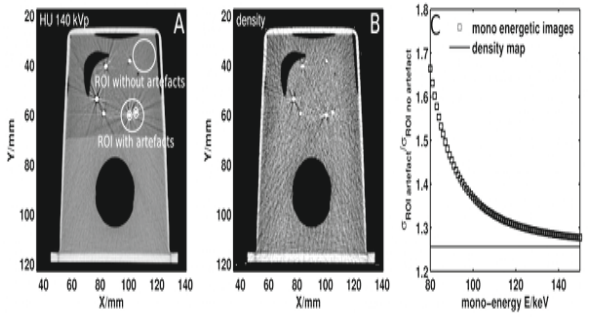

Figure 1

Figure 1A shows the 140 kVp HU (displayed range=[-100 to 200 HU]) with streaking artefacts. Figure 1B shows the density map from ρ-Z decomposition (displayed range=[0.9 to 1.2 g/cc]). Comparing the 140kVp HU image and the density map confirms that DECT provides MAR for seed implants. The magnitude of the metal artefacts in mono energetic images was found to decrease with increasing keV from 70 keV to 150 keV, as can be seen in figure 1C. The ratio of $\sigma_{artefact}/\sigma_{no\text{-}artefact}(E)$ is plotted for the ROIs seen in Figure 1A. The $\sigma_{artefact}/\sigma_{no\text{-}artefact}(E)$ from the density map is plotted as a horizontal line. Our results suggest that the MAR from the density map from ρ-Z decomposition is better than the mono-energetic images, or alternately that the density map corresponds to the best high keV mono-energetic image. The increased noise in the density map can be reduced by optimizing the separation of the high and low kVp spectra.

Conclusions: Mono-energetic images from DECT with a high keV provide MAR in seed implants. The MAR is equivalent to that obtained from the density map. The technique is promising and the impact on dose calculation accuracy will be investigated using Monte Carlo techniques.

OC-0182

Demonstration of real-time, automatic 3D seed & needle localization in brachytherapy using integrated EM tracking

J.A.M. Cunha[1], D.R. Saltiel[1], D. Binnekamp[2], I. Hsu[1], A. Chang[1], J. Pouliot[1]

[1]*University of California (UCSF), Radiation Oncology, San Francisco CA, USA*

[2]*Philips Healthcare, Clinical Innovations Interventional Oncology, Eindhoven, The Netherlands*

Purpose/Objective: Brachytherapy provides one of the best cure rates for the treatment of prostate cancer but is highly skill dependent. An interactive electromagnetic needle navigation system was developed to reduce uncertainty in the implant procedure and expand the capabilities of patient-specific implant techniques.

Materials and Methods: A gelatin phantom was placed inside the work space of a magnet field generator device which tracks the 3D locations of small EM-signal-producing coils. These coils were placed on the end of an endorectal ultrasound probe, upon the probe stepper, and embedded within the wall of a 16 gauge brachytherapy needle. The needle allows passage of a standard prostate brachytherapy seed. These coils provide real-time patient, probe, and needle coordinates. Additionally,the system has a mechanism by which the 3D coordinate and time information provided by the EM tracking device at the moment the seed is deposited in tissue can be automatically recorded.

Experiments were performed to qualitatively determine the usability of the navigation system, as well as to measure the accuracy of the automated seed localization. Multiple seed implants were performed upon a phantom and the automated EM coordinates were compared to the'true' locations, as determined by a CT scan. These two coordinate systems were co-registered using a CT marker placed on the side of the phantom, for which the location was determined using the EM tracked needle by placing the tip upon opposite sides of the marker and averaging the locations' coordinates. The precision of the seed localization is determined by evaluating the differences in relative seed locations within each coordinate system.

Results: The system hardware, interface, and workflow validation experiments were implemented to demonstrate that EM needle tracking can guide implantation of seeds with minimal user expertise. Trials with the EM system have shown,qualitatively, an increase in usability and ease of needle navigation. Preliminary results also indicate the EM tracking seed localization is precise to 2.7 mm (1 sigma).

Conclusions: A system has been developed to assist the placement of radioactive seeds for the treatment of prostate cancer and reduce the dependence on physician skill-level, as well as facilitate skew-line needle arrangements and allow for improved mid-procedure re-optimization based on seed deposition errors. The system will help reduce the number of attempts to bring a needle to the correct seed dropping location as well as facilitate the use of alternative needle pattern for organ sparing. Additionally, automated seed dropping detection will allow the system and user to know immediately the seed location and thereby adjust accordingly. Clinical implementation will be needed to determine the extent of increased precision and reduced trauma.

OC-0183

Independent validation of high dose rate (HDR) brachytherapy source localisation using an EPID

R.D. Franich[1], R.L. Smith[1], M.L. Taylor[1], A. Haworth[2], L.N. McDermott[1], J.L. Millar[3]

[1]*RMIT University, School of Applied Sciences and Health Innovations Research Institute, Melbourne, Australia*

[2]*Peter MacCallum Cancer Centre, Physical Sciences, Melbourne, Australia*

[3]*Alfred Health, Department of Radiation Oncology, Melbourne, Australia*

Purpose/Objective: We have previously shown that a flat panel imager can be used for source position localisation in HDR brachytherapy. Analysis of the EPID image distribution can be used to determine the source position relative to the EPID, but needed to be validated independently. Here we describe a method for the independent validation of source position coordinates determined in the two orthogonal directions parallel to the imager, using a novel projection technique combined with HDR source radiation subtraction.

Materials and Methods: An a-Si EPID (IAS11-19, Varian Medical Systems, Palo Alto, CA, USA), removed from a linear accelerator, was positioned in contact with a rectangular solid water phantom, which included a ball-bearing array, placed against the surface of the imager. Brachytherapy catheters were inserted into grooves cut into a phantom slab at a distance of 50 mm from the imager surface. A mobile x-ray unit was set up at a relatively large distance (1500 mm) from the imager. Radio-opaque x-ray source position markers were inserted into the catheters and a projection image acquired using the external x-ray source and the EPID. A marker was removed and the Ir192 brachytherapy source was driven to 5 programmed dwell positions, at 10 mm steps, corresponding to the expected x-ray marker positions. At each dwell position two images were acquired: the first capturing only the radiation emitted by the Ir192 source, while the second image acquired also contained an exposure from the external x-ray system. Using image subtraction, the position of the projection of the physical Ir192 source could be determined and correlated with the marker projections (See Figure 1). To account for beam divergence effects, the distance of each projection from the central axis (CAX) of the external x-ray beam was determined. A stereotactic angiographic localisation frame was used as a set of known orthogonal pairs of radio-opaque markers, with the CAX determined by co-location of the perpendicular pair in the image.

Results: The centroid coordinates of marker and source projections were derived and used to calculate object locations *via* geometric back-projection. Marker locations and the HDR source itself, identified using the subtraction method described here, were determined to within ± 0.4 mm (± half of the pixel size) at each programmed dwell position. Derived source positions matched the marker positions.